VICTORIA UNIVERSITY
MELBOURNE AUSTRALIA

Numerical analysis of airflow and particle deposition in multi-fidelity designs of nasal replicas following nasal administration

Numerical analysis of airflow and particle deposition in multi-fidelity designs of nasal replicas following nasal administration

Zhiwei Shen [a], Jingliang Dong [b,c,*], Liam Milton-McGurk [d], Xinyu Cai [a], Hanieh Gholizadeh [e], Hak-Kim Chan [f], Ann Lee [a], Agisilaos Kourmatzis [d], Shaokoon Cheng [a]

[a] School of Engineering, Faculty of Science and Engineering, Macquarie University, Sydney, NSW 2109, Australia
[b] Institute for Sustainable Industries & Liveable Cities, Victoria University, P.O. Box 14428, Melbourne, VIC 3011, Australia
[c] First Year College, Victoria University, Footscray Park Campus, Footscray, VIC 3011, Australia
[d] School of Aerospace, Mechanical and Mechatronic Engineering, The University of Sydney, Sydney, NSW 20061, Australia
[e] Division of Pulmonary, Allergy and Critical Care Medicine, Department of Medicine, University of Pittsburgh, Pittsburgh, Pennsylvania, USA
[f] Advanced Drug Delivery Group, Sydney Pharmacy School, Faculty of Medicine and Health, The University of Sydney, Sydney, NSW, Australia

ARTICLE INFO

ABSTRACT

Background and Objective: An improved understanding of flow behaviour and particle deposition in the human nasal airway is useful for optimising drug delivery and assessing the implications of pollutants and toxin inhalation. The geometry of the human nasal cavity is inherently complex and presents challenges and manufacturing constraints in creating a geometrically realistic replica. Understanding how anatomical structures of the nasal airway affect flow will shed light on the mechanics underpinning flow regulation in the nasal pharynx and provide a means to interpret flow and particle deposition data conducted in a nasal replica or model that has reduced complexity in terms of their geometries. This study aims to elucidate the effects of sinus and reduced turbinate length on nasal flow and particle deposition efficiencies.

Methods: A complete nasal airway with maxillary sinus was first reconstructed using magnetic resonance imaging (MRI) scans obtained from a healthy human volunteer. The basic model was then modified to produce a model without the sinus, and another with reduced turbinate length. Computational fluid dynamics (CFD) was used to simulate flow in the nasal cavity using transient flow profiles with peak flow rates of 15 L/min, 35 L/min and 55 L/min. Particle deposition was investigated using discrete phase modelling (DPM).

Results: Results from this study show that simplifying the nasal cavity by removing the maxillary sinus and curved sections of the meatus only has a minor effect on airflow. By mapping the spatial distribution of monodisperse particles (10 μm) in the three models using a grid map that consists of 30 grids, this work highlights the specific nasal airway locations where deposition efficiencies are highest, as observed within a single grid. It also shows that lower peak flow rates result in higher deposition differences in terms of location and deposition quantity, among the models. The highest difference in particle deposition among the three nasal models is ~10%, and this is observed at the beginning of the middle meatus and the end of the pharynx, but is only limited to the 15 L/min peak flow rate case. Further work demonstrating how the outcome may be affected by a wider range of particle sizes, less specific to the pharmaceutical industries, is warranted.

Conclusion: A physical replica manufactured without sections of the middle meatus could still be adequate in producing useful data on the deposition efficiencies associated with an intranasal drug formulation and its delivery device.

1. Introduction

A comprehensive understanding of what factors affect fine particle transport and deposition in the human airway is important to ascertain the efficacies of aerosol drug delivery [1,2],. Understanding the total and local/regional deposition of particles is important, as depending on the mechanisms of action and working principle of a given drug, a particular level and distribution of particle deposition in the nasal

airway is typically desired. For example, nose-to-brain drug delivery has been widely regarded as a plausible method to bypass the blood brain barrier and to deliver drugs directly to the brain to treat neurological disorders [3–5], and so maximizing drug delivery to the olfactory region for this treatment modality would be required. Interest in developing intranasal drugs has also surged since the global COVID-19 pandemic [6] because vaccinations could potentially be delivered via the intra-nasal route [7–9] Here the mucosa consists of high blood vessel density and presents immunocompetent cells that can potentially help to provide additional protection against viruses. Improved knowledge of fine particle delivery and deposition in the human nasal airway is also highly valuable for the assessment of health hazards related to pollution and toxin inhalation.

Studies on fine particle transport in the nasal airway have been largely undertaken by computational modelling developed using computational fluid dynamics (CFD). In vitro studies to study particle deposition in human nasal airway replicas are extremely valuable, albeit rarer in the literature. Developing a geometrically realistic cast of the nasal airway for in-vitro experiments can be challenging, given the nasal geometry's manufacturing constraints, especially when criteria to clean and maintain the cast are needed. The above may indicate why current replicas on the market do not accurately represent the human nasal airway geometry. While the Koken nasal cast (Koken Co., Tokyo), consists of many physiologically realistic features, including the geometrical complexity of some sections of the nasal turbinate structure, it comprises a flat surface on one side of the nasal airway, which is likely to affect flow dynamics significantly. Indeed, while the Koken nasal cast design offers a high degree of usability and maintenance, this has come at the expense of removing some seemingly important anatomical details of the nasal airway. Another example is the Alberta Nasal Inlet (The Aerosol research lab of Alberta, Edmonton, Alberta). The replica is relatively easy to clean and maintain, as the geometry has been significantly idealized, and details of the human nasal airway anatomical structures have not been recapitulated in their entirety. When developing a nasal replica to study the transport and deposition of particles, it is necessary to ensure that any simplification of the cast will not produce misleading deposition data such that the results are significantly different when the complete human nasal airway geometry is considered. An in-depth analysis of this may be adequately performed using CFD to show what anatomical features of the nasal airway can be safely sacrificed or how data may be interpreted within well-defined constraints when using a geometrically simplified nasal cast.

Inthavong et al. [10] investigated the deposition of nasal spray particles using steady-state flow and mono-disperse particles (10 μm and 20 μm). The particles were released as a cone spray administered at a distance from the entrance of the nasal cavity. The study showed that deposition efficiency for the 10 μm particles was as high as 63.2% at the front of the nasal cavity and demonstrated clearly that variations in the spray cone angle of nasal spray designs could substantially impact regional particle deposition within the nasal chamber. The study further suggests that design approaches to ensure adequate insertion length could be useful in achieving precise drug delivery to targeted areas within the nasal airway. Zare et al. [11] used an angled tip nasal spray to explore the impact of the released angle on particle deposition within the inferior meatus of the nasal airway under steady-state flow. Their investigation showed that the angled tip spray demonstrated that particle can be delivered to the inferior meatus without tilting head, which was not the case with the straight nasal spray. Tong et al. [12] investigated the impact of nasal-spray nozzle orientations on the deposition of monodisperse particles in a geometrically realistic airway model reconstructed from CT scan images. Similar to the conclusion of Inthavong et al. [10], the results of their study verified that spray nozzle orientation is a critical factor underpinning a device's efficacy and purported that a nasal device aligned with the nostril's centre axis is the most efficient protocol to ascertain higher delivery compared with pointing upwards and downwards. While using steady-state flow to model nasal sprays is adequate, less is known about flow dynamics in the nasal airway under physiologically realistic respiratory flow conditions.

In this study, we aim to understand how simplifying the nasal geometry may affect the flow field and particle deposition in the airway. Specifically, we will remove the sinus and some sections of the turbinate. A key novelty of this current work is that we have controlled the flow conditions and general geometry of the nasal airway, and have systematically elucidated how the absence of key anatomical features may or may not affect particle deposition. The study's overarching goal is to clarify whether the above simplifications would drastically change particle deposition results and flow field in the airway. This work is important for two primary reasons. First, if simplifying the nasal geometry will not result in any drastic change in flow field or deposition outcome, this information can guide the design and manufacturing of future nasal replicas, as removing certain aspects of the nasal turbinates would significantly improve their manufacturability from the casting perspective. Second, if some changes are noted between the simplified and the non-modified airway, knowledge produced from this work would be needed to interpret the test results of future nasal drug delivery products or respirable hazardous fine particles when tested using the simplified nasal airways.

2. Methods

The research was authorized by the Human Research Ethics Committee of Macquarie University and was carried out in compliance with the principles of the Declaration of Helsinki. The subject volunteer provided informed written consent before participating in the study.

2.1. Nasal airway imaging and reconstruction

A healthy male (28 years old) with no prior history of nasal diseases volunteered for the study. MRI was performed on the subject. The subject was requested to lie supine and breathe quietly through the nose. A pad was placed around the volunteer's head to minimise head motion during the scan. Communication was maintained with the subject through an intercom and buzzer. The following MRI parameters were used to obtain the isometric anatomical images: field of view of 256 mm and a matrix size of 256 × 256 (with a pixel size of 1 mm × 1 mm), a repetition time of 6.8 ms, an echo time of 3 ms, a scan resolution of 144 × 108, and a slice thickness of 1 mm. The total scan time was 6 min.

Three nasal airway models were reconstructed from a single set of MRI data using 3D slicer (www.slicer.org). The first model - the base model, consists of the entire nasal airway and maxillary sinus. The model was modified to produce the second model, where the maxillary sinus was removed. The third model was created by shortening the turbinate structure by removing the meatus bends. The three fidelity models are shown in Fig. 1. It is worth noting that the turbinate resection is not performed from an in vivo clinical perspective, but rather from an in vitro manufacturing point of view during model casting. In essence, it is extremely difficult to completely remove support water-soluble materials within the distal curved meatus regions, thus the modified turbinate model was adopted to mimic the nasal replica structure with reduced meatus space. The nasal models were imported to Geomagic wrap (Artec 3D, Senningerberg, Luxembourg) and dissected into four
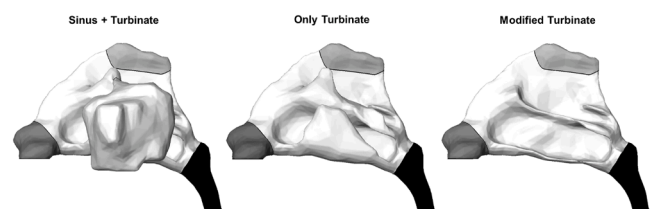

Fig. 1. Side view of three fidelity models.

main sections for detailed analysis (See Fig. 2). These sections are the (i) Vestibule, (ii) Nasal main passage, (iii) Olfactory region and (iv) Nasopharynx. Three different planes were defined at the anterior, middle, and posterior sections of the nasal airway models to further analyse the flow field in the nasal airway. The computational models were imported into ANSYS ICEM-CFD (ICEM CFD Engineering, Ansys 2019 R3, Canonsburg, Pennsylvania) and ANSYS FLUENT (Ansys 2019 R3, Canonsburg, Pennsylvania) to generate the surfaces and polyhedral meshes. Based on mesh convergence analysis (See supplementary data), the optimum mesh density was determined to be 1.3 million with 5 inflation layers, after a series of mesh independence tests.

2.2. Governing equations

Eq. (1) was used to analyse the Reynolds number for all the models. The air density (ρ) and dynamic viscosity (μ) were prescribed as 1.225 kg/m³ and 1.825×10^{-5} kg/ms, respectively. The peak flow rate of the inhalation flow was used to determine the velocity (v), and the characteristic length (L) was determined from the outlet of the nasal airway.

$$Re = \frac{\rho v L}{\mu} \tag{1}$$

SST K-ω turbulence model [13] was used as the numerical scheme for the simulations. The airflow within the nasal airway is considered both incompressible and isothermal. The continuity and momentum equations are presented in Eqs. (2) and (3), respectively, where U is the mean flow velocity (m/s), t is the time (s), p is the pressure (Pa), ρ is the density (kg/m³), and v is the velocity vector (m/s) [14]

$$\frac{\partial U_i}{\partial x_i} = 0 \tag{2}$$

$$\frac{\partial U_i}{\partial t} + U_j \frac{\partial U_i}{\partial x_j} = -\frac{1}{\rho}\frac{\partial p}{\partial x_i} + \frac{\partial}{\partial x_j}\left[(\nu + \nu_T)\left(\frac{\partial U_i}{\partial x_j} + \frac{\partial U_j}{\partial x_i}\right)\right] \tag{3}$$

The simulation of particle transport was guided by the governing equation shown in Eq. (4), which is the standard discrete phase modelling (DPM) formulation.

$$\rho_P d_p \frac{d^2 x_P}{dt^2} = \frac{3}{4}\rho C_D (v - v_P)|v - v_P| + \rho_P d_P g \tag{4}$$

Where g is the gravity vector with a value of 9.81 N/kg, ρ_P is the particle density (kg/m³), d_P is the particle diameter (m), x_P is the particle displacement (m), C_D is the drag force coefficient, and v is the velocity vector (m/s).

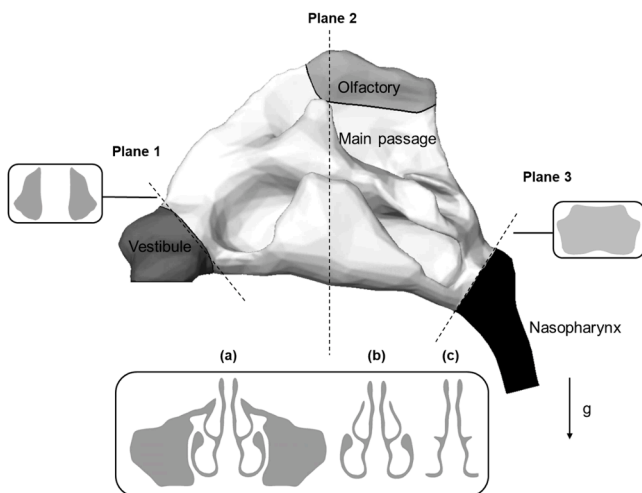**Fig. 2.** Nasal airway models used for computation modelling (a) Complete airway model, (b) Only Turbinate model and (c) Modified Turbinate model.

2.3. Boundary conditions

The models created were solved using ANSYS FLUENT. Double precision and parallel processing with six processors were selected. A transient flow simulation was performed in all three models using a sinusoidal breathing profile with peak flow rates of 15 L/min, 35 L/min, and 55 L/min and a cycle time of 4 s. These flow rates are physiologically realistic and meaningful. For example, 15 L/min represents tidal breathing, and 55 L/min represents deep inhalation. The breathing profiles are shown in Fig. 3.

Particle deposition was simulated in the nasal model under steady flow conditions of 15 L/min, 35 L/min, and 55 L/min. The reason for using the steady flow condition in our investigation of particle deposition is to observe its behaviour specifically at the peak flow rate. The aim of this simulation was to investigate how particles were deposited in the three different nasal models. Monodisperse particles, commonly used in existing work [E.g. [12,15]], also used in simulations presented in this current work, have a diameter of 10 μm. The particle density value used was 1514 kg/m³. The DPM boundary condition was set to "escape" at the inlet and outlet, while "trap" was prescribed at the walls. The flow was prescribed at the outlet (nasopharynx), and pressure at the inlet (nostril) was defined as zero.

3. Results

3.1. Flow field results

15 L/min peak flow rate case (Fig. 4) - Results in the top row of Fig. 4 show the velocity contour at plane 1 (nasal vestibule) extracted at 1 s for the 15 L/min peak flow rate case. The velocity field is similar for all three models, with magnitudes in the range 0 to ∼ 2.68 m/s. Despite the fairly large differences in the overall airway geometries, the velocity field in this region appears unaffected by these differences. The middle row shows the velocity contour at plane 2. The maximum velocity in the model with maxillary sinus is ∼ 1.79 m/s. Not surprisingly, due to the limited connection between the turbinate and the sinus, flow in the sinus region is small and appears negligible. There is a subtle change in velocity between the middle meatus and the sinus cavity, and the magnitude is ∼ 0.45 m/s. Other regions of the airway that have almost insignificant or no flow, similar to those observed in the sinus, appear to be at the tip of the turbinates, as illustrated by the rectangular insets. It is also worth noting that velocity magnitude appears to fluctuate along the turbinate passageway in the cranial-caudal direction. For example, for this subject-specific model, the flow magnitude along the turbinate oscillates between 1.79 and 0.45 m/s. Whether the above observations are ubiquitous in other human subjects and present a unique mechanism of the nasal airway to regulate flow is unclear and merits further investigation. Based on the results at plane 2, there are indistinguishable differences in the velocity magnitude between the complete airway model
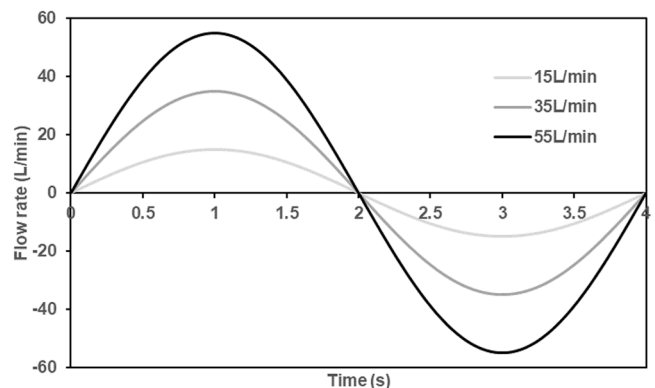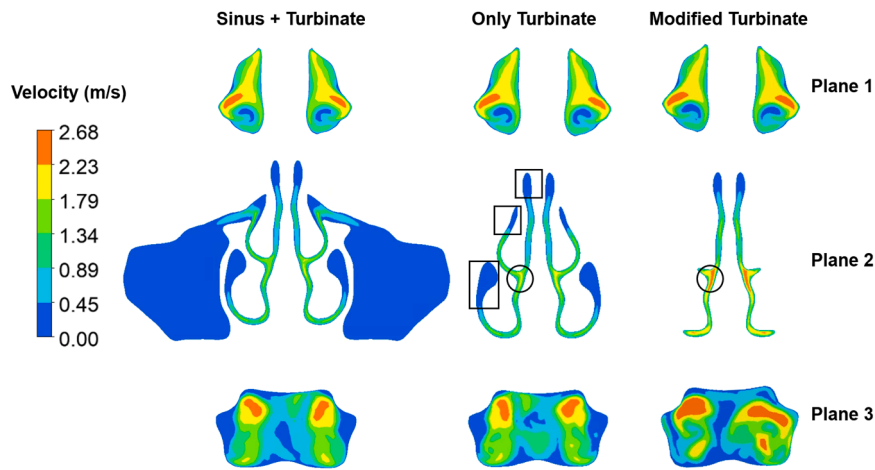

Fig. 3. Breathing profiles.

Fig. 4. The velocity contour of the three airway models, simulated with a transient flow with a peak flow rate of 15 L/min.

and the turbinate-only model. In the modified turbinate model, the velocity at the intersection between the middle meatus and turbinate passageway (see circle inset) is ~1.5 times higher than the other two models and is ~ 2.68 m/s. Further discussions on cases simulated with the respiratory flow with higher peak flow rates will show how these values may be affected.

35 L/min peak flow rate case (Fig. 5) - The velocity contour pattern in all airway models simulated with this flow rate condition is somewhat similar to those of the 15 L/min cases, with only a few minor differences at some airway locations.

55 L/min peak flow rate case (Fig. 6). In the 55 L/min case, the velocity fields at the nasal vestibule are very similar across all three models, and are more similar to each other than in the lower peak flow rate cases. The maximum velocity here is ~ 8.68 m/s, which is the same across all three nasal models, and is about 1.3 times higher than to the 35 L/min cases. Despite simulating a higher flow rate than previous cases, the olfactory and the distal ends of the nasal meatus, as expected, still receive minimal ventilation rates. This observation purports that particle deposition in that region would require imparting momentum to particles from other regions in the nasal cavity and needing favourable trajectories that could lead to diversion to the olfactory cleft.

Fig. 7 characterizes the velocity along the turbinate passageway at plane 2 and when the peak flow rate occurs. To undertake this analysis, 8 locations are identified and spread evenly along plane 2, and the spatial average velocity is computed at these locations. The bottom panel in the figure (Panel B), shows the results for the 3 models simulated with

different flow conditions (e.g. the 15 L/min, 35 L/min and 55 L/min peak flow rate cases). The data shows that velocity fluctuates somewhat along the passageway, and velocity at the bottom of the passage (P1 and P7) is ~ 33% less than the highest velocity, which occurs at P3 near the middle meatus. Velocity generally decreases in the cranial direction beyond P3. A notable observation here is that beyond P3, and towards the olfactory region, except for the low flow rate case, the results are similar for the 3 different nasal models despite having some significant differences in the nasal geometry. Between P4-P6 for 35 L/min and 55 L/min, the velocity is similar for all models at the given flow rate. This could suggest there is a potential threshold effect with respect to the middle turbinate length, such that when exceeded, the influence of turbinate geometry on the velocity is reduced in this region.

3.2. Particle deposition results

The following section discusses the particle deposition in the models. This is summarised in Table 1, which gives the percentage of particles that deposit locally in four different regions of the airway, and the remaining percentage that exit through the outlet. Since this is a monodisperse flow with spherical particles all of the same density, the number, mass and volume based deposition fractions are equivalent, and are given by,

$$DE\% = \frac{number\ of\ deposited\ particles}{number\ of\ injected\ particles} \times\ 100\% \tag{5}$$
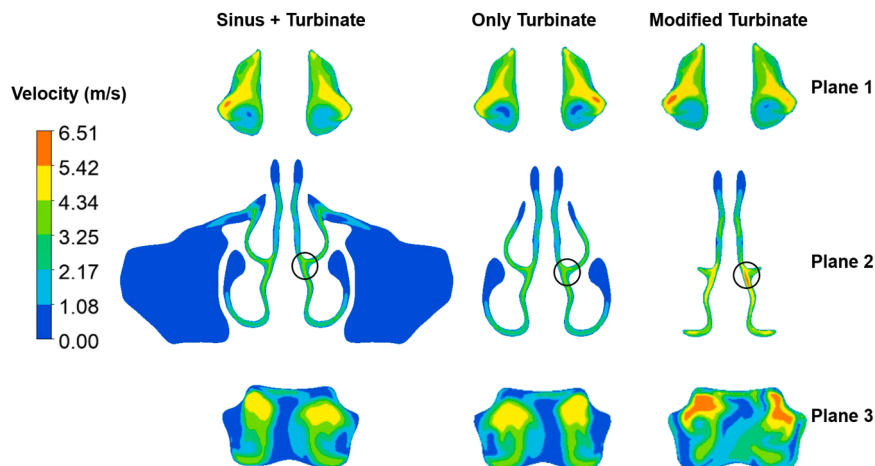

Fig. 5. The velocity contour of the three airway models, simulated with a transient flow with a peak flow rate of 35 L/min.
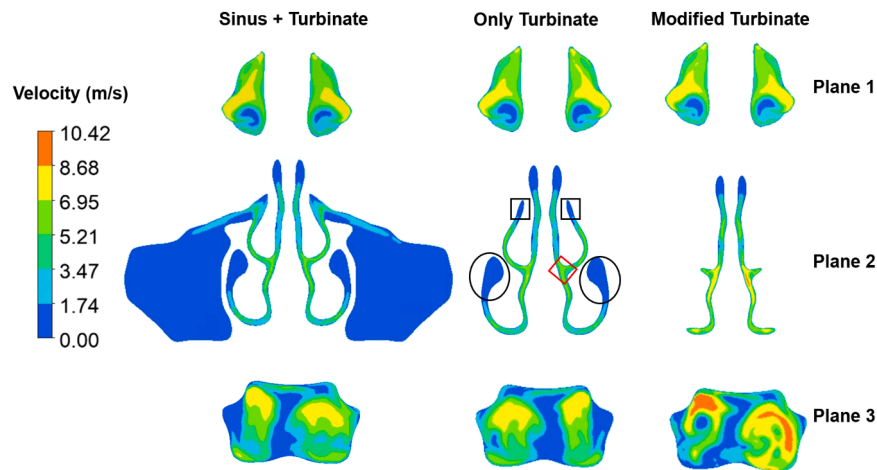
Fig. 6. The velocity contour of the three airway models, simulated with a transient flow with a peak flow rate of 55 L/min.
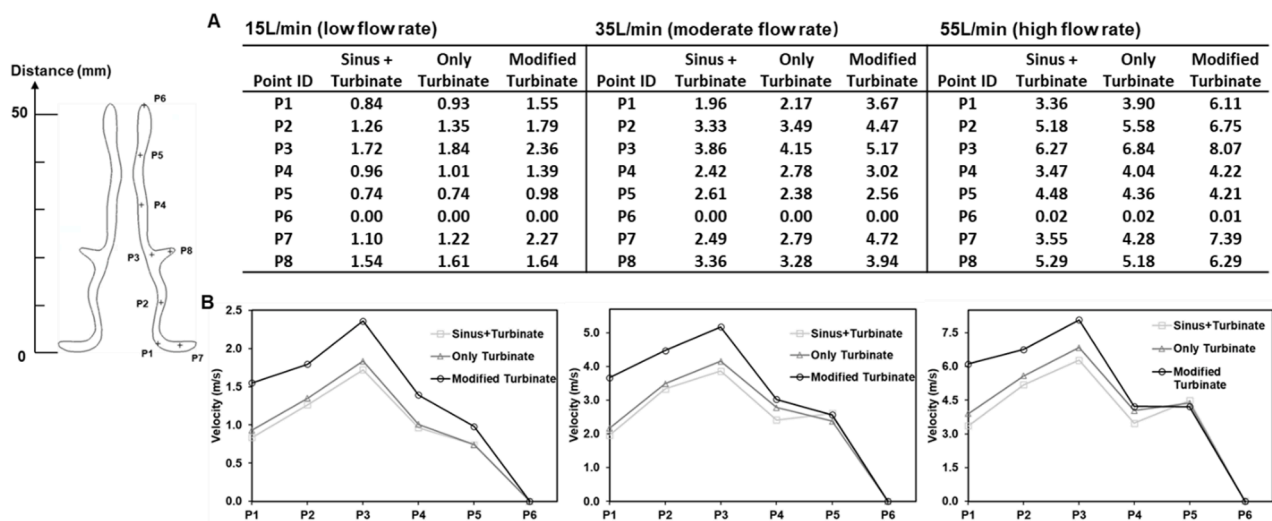

Fig. 7. Velocity changes along the main passage in the middle plane in three different airway models.

Table 1
Regional deposition efficiency of 10 μm particles in nasal models with varying geometries.

55 L/min	Sinus + Turbinate	Only Turbinate	Modified Turbinate
Main passage	**98.41%**	**98.23%**	**98.02%**
Vestibule	**1.56%**	**1.74%**	**1.69%**
Sinus	**0.00%**	**0.00%**	**0.00%**
Pharynx	**0.01%**	**0.03%**	**0.10%**
Escape	**0.02%**	**0.00%**	**0.01%**
15 L/min	Sinus + Turbinate	Only Turbinate	Modified Turbinate
Main passage	**57.17%**	**46.73%**	**51.28%**
Vestibule	**2.53%**	**2.81%**	**3.01%**
Sinus	**0.56%**	**0.00%**	**0.00%**
Pharynx	**16.40%**	**25.51%**	**24.40%**
Escape	**23.34%**	**24.91%**	**21.31%**
35 L/min	Sinus + Turbinate	Only Turbinate	Modified Turbinate
Main passage	**94.62%**	**95.78%**	**96.36%**
Vestibule	**1.52%**	**1.64%**	**1.95%**
Sinus	**0.03%**	**0.00%**	**0.00%**
Pharynx	**2.88%**	**2.57%**	**1.61%**
Escape	**0.95%**	**0.01%**	**0.08%**

While the total deposition is similar for each model at a given flow rate, there are notable differences in the local deposition between the models. For instance, particle deposition at the pharynx region appears to be the most affected by the presence of sinus. At a low flow rate of 15 L/min, deposition in the pharynx is the lowest for the complete airway model. The situation changes at 35 L/min, where *DE%* at the pharynx is the highest in this model. At 55 L/min, it becomes negligible and the number of particles deposited at this region is only about 0.01%. While only 3 flow rates are investigated, it is apparent that particle deposition at the main nasal passage increases with increasing flow rate and appears to follow a non-linear trend. That is, the marginal increase in deposition is reduced as the flow rate continues to rise, with *DE%* in this region nearing 100% at 55 L/min. Given that particles not trapped by the nasal main passage will migrate downstream, deposition also occurs at the pharynx, which presents the final gateway to trap particles before they exit. Another interesting observation is that deposition in the vestibule is consistent for all three models and across flow rates.

Overall and regional particle deposition (Fig. 8 and 9) - Fig. 8 shows the locations where particles have deposited by the end of the simulations. Although there are some small local differences between the three models at a given flow rate, the broad deposition pattern is similar for all models. For this subject-specific model, the flow rate appears to be the most significant factor that affects how the particles are deposited (as opposed to the more minor influence of nasal geometry). It affects the trajectory of the particles moving through the nasal cavity, with higher flow rates appearing to increase the likelihood that particles reach the superior section of the nasal airway, such as the olfactory region.
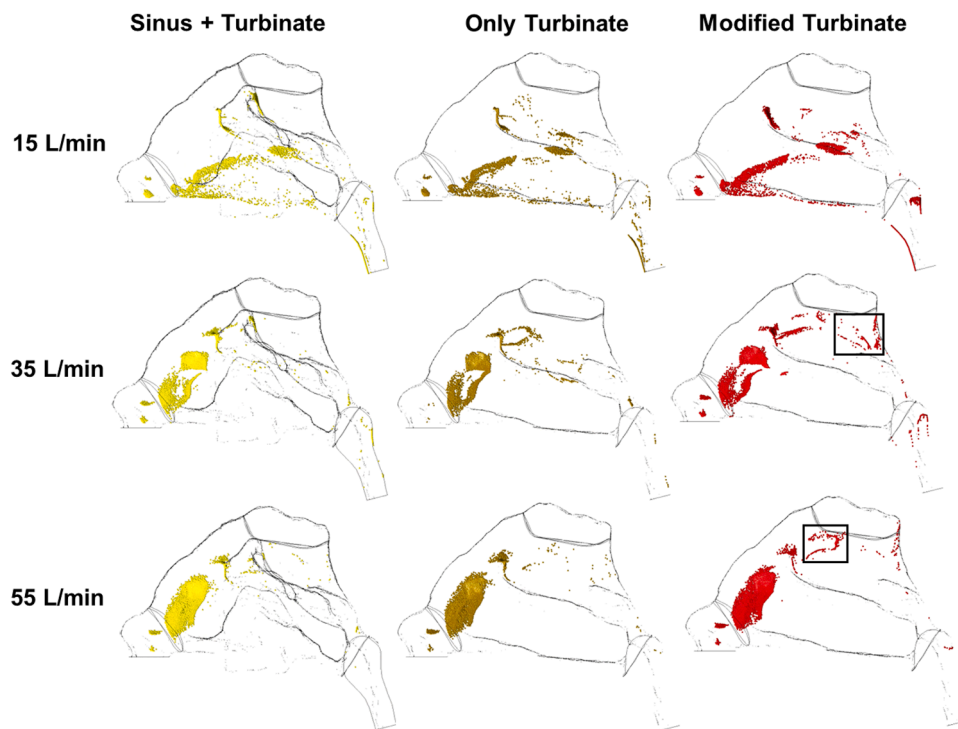
5

Fig. 8. Overall particle deposition simulated with 10 μm size particles.
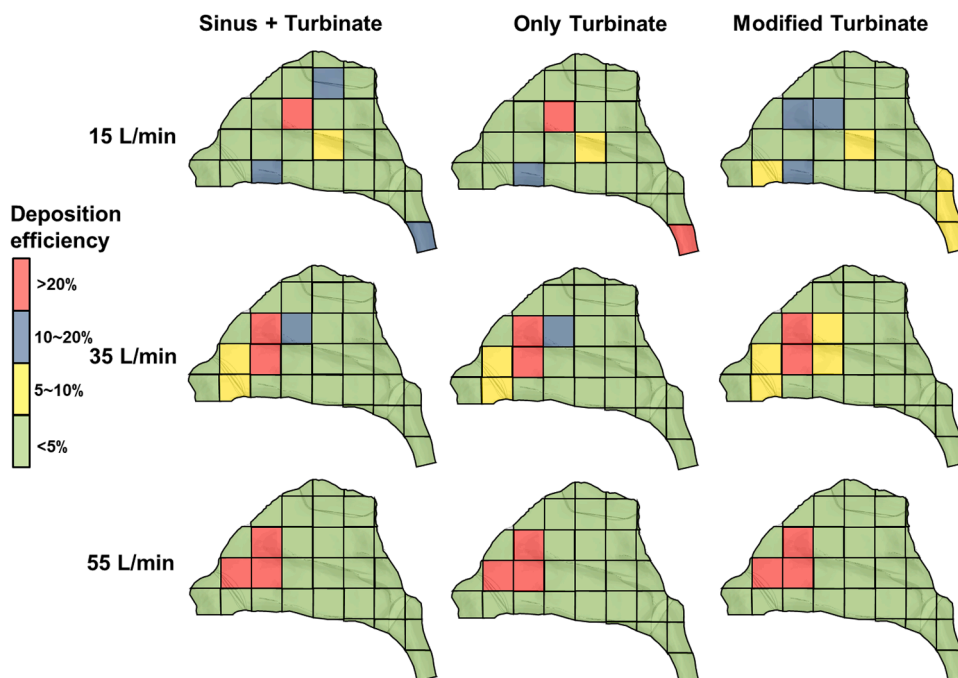

Fig. 9. Particle deposition map for all flow rate cases simulated with 10 μm size particles.

However, interestingly, when comparing the three models in terms of their efficacy in delivering particles to regions adjacent to the olfactory, it appears that the modified turbinate model may tend to overestimate deposition data. This should be taken into consideration when using the model or it's physical replica to study nasal-brain drug delivery. There also appear to be some airway regions where particles only deposit in the modified turbinate model (see rectangular insets). To understand whether these differences will have any implications on drug delivery performance, the following section consolidates the number of particles deposited across the nasal airway models to shed further light on the potential limitations of using simplified models of the nasal airway.

The nasal airway models were dissected into 30 different regions to form a grid map with a grid size of 11 mm x 11 mm, as shown in Fig. 9. Particle deposition bounded by each grid was analysed, and regions with less than 5% deposition are highlighted green. Regions that have particle deposition between 5 – 10% are highlighted yellow, regions with particle deposition between 10 – 20% are highlighted blue and regions with particle deposition in excess of 20% are highlighted red. In essence,

the map provides insights into where deposition data may be acceptable when a modified turbinate model is used, such that their results are similar to the complete airway model. The results presented here suggest that interpreting the data from the different nasal models would rely on the range of flow rates investigated. For example, at higher flow rates, such as the 55 L/min cases investigated in this study, deposition is comparable across the models, and using a simplified nasal airway may become increasingly feasible and meaningful. For the low inhalation flow rate, the deposition results remain useful for all the models except for the beginning of the middle meatus and pharynx section, where an observed difference of ~10% in those sections has been determined.

4. Discussion

A nasal cast that enables accurate deposition data to be obtained can be of paramount importance to the success of intranasal drug delivery-related products. These measurements can be misleading without a geometrically realistic nasal cast model. In addition, for practical reasons, such as the need to perform repeated tests in the field of inhaled drug delivery, a cast that can be easily cleaned, maintained and assembled for use would be a convenient feature. From the mechanical design perspective, achieving this may need to come at the expense of sacrificing certain geometrical details of the nasal airway. It is hence important to understand the implications and limitations of a simplified airway model. To the best of the author's knowledge, this is the first work describing how a nasal airway with reduced complexity of the turbinate structure may produce meaningful deposition data that corresponds well with a complete nasal airway. Results from this study suggest that based on the particle size and flow conditions investigated, a modified turbinate nasal airway is likely adequate to study particle deposition.

Shrestha et al. [16] utilized a CT scan of a 75-year-old male with chronic rhinosinusitis to create a 3D computational model of a nasal cavity and sinuses after performing virtual surgery on the model. They also simulated a sinusoidal breathing profile similar to the one used in this study. The velocity magnitude during the peak inhalation rate was similar to the results obtained in this study, being ~5.5 m/s, which is only 10% greater than the results of our 35 L/min peak flow rate case. The location that exhibits the highest velocity magnitude at plane 2 was also at the middle meatus, similar to what has been demonstrated in this current work. Given that the human airways are extracted from two different individuals (this current study and the work of Shrestha et al. [16]), it shows that the geometry of the nasal airway presented in this current study and Shrestha et al. [16] is similar for the turbinate structures and the overall nasal geometry. The fact that velocity at the mid-turbinate region is the highest, which agrees with the present study, also suggests that this may be common in humans. One of the key differences, however, is that as seen in the velocity contour presented, the velocity magnitude at plane 2 ($t = 1$ s) is generally higher than what Shrestha et al. [16] have shown ($t = 0.825$ s), which is likely because of the slight difference in respiratory flow profile used.

In this current study, 10 µm size particles are used, which is similar to what has been used in some existing work. Results obtained in this current study are in strong agreement with those reported by Tong et al. [12], who simulated 10 µm size particles and showed that at high flow rates, there was a complete deposition (approx. 100%) of particles in the nasal airway. The different nasal airway geometries between Tong et al. [12], and this current work flag potential discrepancies in regional deposition one may expect when different nasal airways are investigated. Even though the overall deposition is the same, particle deposition at the anterior of the vestibule is ~20% higher in Tong et al. [12] than in this current work. This observation highlights the potential importance of the nose arch and the geometry of the vestibule between individuals, which may have significantly affected the regional deposition behaviour in the nasal airways, and this merits further investigation. The particle deposition efficiency of nasal sprays was also

investigated by Calmet et al. [17] using large eddy simulation (LES). Despite using different particle sizes, results from Calmet et al. [17] are more in line with the outcome produced in this current work than those produced by Tong et al. [12] Similar to this current study, spray through the nose was prescribed as a cone, but with a half-cone angle of 17 °, break length of 5 mm, velocity of 49 m/s, and peak volumetric flow rate of 60 L/min. The results from Calmet et al. [17] showed that the majority of polydisperse particles with a median volume diameter of 25.5 µm were deposited within the nasal cavity, again with nearly 100% deposition efficiency. The deposition efficiencies were found to be 3.4%, 96.5%, and 0.01%, at the anterior, middle and posterior regions respectively. These findings align exceptionally well with our results, where most particle deposition is found at the main passage. Calmet et al. [17] also performed a physical experiment using a rigid nasal cast, with similar geometries as their computational model, albeit not having the sinus. The experimental results were in fairly strong agreement with the deposition at the main passageway, where 87% of particles have been observed, which is ~ 10% lower than what has been simulated by the computational models. One of the explanations could be related to the 2-way coupling interaction between the particles and flow, which has not been included in the current computational models. This plausible argument is supported by simulations preformed in Kolanjiyil et al. [18] Another noteworthy work was produced by Inthavong et al. [19], who investigated particle deposition efficiency based on the release of particles using a solid cone profile. With a flow rate of 20 L/min and using 15 µm monodisperse particles, they recorded 100% deposition of particles at approximately the same location as our airway. This outcome again supports the concept that it is challenging for a substantial proportion of particles to be transported to the posterior region of the nasal cavity at high flow rates.

There are a few inherent limitations to the study design that should be considered when interpreting the findings of this study. Firstly, the nasal geometry is extracted from a single individual. Larger differences in deposition data could be potentially observed when the anatomical details (e.g., sections of the turbinates) are removed from the nasal airway of other individuals. While this could be the case, it is important to note that we have compared the results of this current work with other existing research which have performed simulations based on similar flow and aerosol administering conditions. The comparison, as discussed, suggests that variances in nasal geometries between humans though critical, are likely to yield similar deposition patterns as observed in this current work. As noted, future studies delineating the effects of the vestibule and how it controls deposition behaviour downstream of the airway are warranted, as it appears to be a key region that could affect the regional deposition of particles. Another limitation of this study design is that 10 µm monodisperse particles are used. This particle size is used because this is particle size commonly used for nasal spray related studies, which is important to provide us with the means to compare our data with published work. Tong et al. [12] investigated the deposition of particles sizes 15 and 50 µm, and showed that with larger particle size, a notable increase in deposition at the anterior portion of the nasal airway, primarily the vestibule is observed. According to Tong et al. [12], this is related to the impact of inertia relating the size of the particles. In a separate study conducted by Schroeter et al. [20] who studied 10 and 20 µm size particles, they showed that similar to Tong et al..'s [12] results, it was more difficult for the larger particles to depart from the airflow streamline due to inertia, and this resulted in higher deposition at the anterior section of the nasal cavity. Although our current investigation did not simulate larger particle sizes as the focus of the work is to elucidate the implications of simplified turbinate structures, existing published work as discussed above suggests that it is likely that more particles will be deposited at the vestibule when larger particles size is simulated. Interestingly, the work of Calmet et al. [17] shows that, despite using polydisperse particles, the particle deposition results are somewhat similar to this current study. Calmet et al. [17] proposed that spray parameters such as the injection velocity,

breakdown length, and injection angle are all important factors, in addition to flow profile and particle sizes, that determine the fate of particle deposition in the complex nasal airway. Their study revealed that the deposition patterns in the anterior and middle regions are strongly correlated with the injection angle and breakup length. In contrast, the posterior deposition appeared to be predominantly affected by the injection velocity, highlighting the crucial role of controlling spray parameters to realize particle deposition at specific regions of the nasal airway. Understanding how transient inhalation flow may affect particle deposition behaviour as compared to steady state flow is also important. Unfortunately, studies in this area remain scarce, and integrating it in future work is necessary to further improve knowledge in particles transport and their deposition in the nasal airway under physiological realistic conditions.

5. Conclusions

Results from this work suggest that the absence of the maxillary sinus in a physical replica designed to observe and quantify particle deposition is physically meaningful. In addition, removing the curved sections of the meatus (in the coronal plane) also produced minor changes to the velocity contour. Although there was a slight increase in the velocity magnitude in the middle meatus, this appears to have little impact on particle deposition at the main nasal passageway, and only a few grid regions (Fig. 9) have been identified as significantly different. Hence, a physical replica manufactured without sections of the middle meatus could still be adequate in producing useful data on the deposition efficiencies associated with an intranasal drug formulation and its delivery device.

Declaration of Competing Interest

All authors report no potential competing interests. The content of the manuscript has not been published or submitted for publication elsewhere, and all authors have approved the manuscript for the submission to Computer Methods and Programs in Biomedicine.

Supplementary materials

Supplementary material associated with this article can be found, in the online version, at doi:10.1016/j.cmpb.2023.107778.

References

[1] A. Kourmatzis, S. Cheng, H.K. Chan, Airway geometry, airway flow, and particle measurement methods: implications on pulmonary drug delivery, Expert Opin. Drug Deliv. 15 (3) (2018) 271–282.

[2] T. Mekonnen, et al., A review of upper airway physiology relevant to the delivery and deposition of inhalation aerosols, Adv. Drug Deliv. Rev. 191 (2022), 114530.

[3] C.L. Graff, G.M. Pollack, Nasal drug administration: potential for targeted central nervous system delivery, J. Pharmaceut. Sci. 94 (6) (2005) 1187–1195.

[4] T.P. Crowe, W.H. Hsu, Evaluation of recent intranasal drug delivery systems to the central nervous system, Pharmaceutics 14 (3) (2022) 629.

[5] S.V. Dhuria, L.R. Hanson, W.H. Frey, Intranasal delivery to the central nervous system: mechanisms and experimental considerations, J. Pharmaceut. Sci. 99 (4) (2010) 1654–1673.

[6] Z. Hoseini-Tavassol, et al., Natural derived nasal spray; a proposed approach for COVID-19 disease control, Infect Disord. Drug Targ. 21 (8) (2021), e160921191568.

[7] A.O. Hassan, et al., A single-dose intranasal ChAd vaccine protects upper and lower respiratory tracts against SARS-CoV-2, Cell 183 (1) (2020) 169–184, e13.

[8] R.G. King, et al., Single-dose intranasal administration of AdCOVID elicits systemic and mucosal immunity against SARS-CoV-2 and fully protects mice from lethal challenge, Vaccines 9 (8) (2021) 881.

[9] X. An, et al., Single-dose intranasal vaccination elicits systemic and mucosal immunity against SARS-CoV-2, iScience 24 (9) (2021), 103037.

[10] K. Inthavong, et al., Optimising nasal spray parameters for efficient drug delivery using computational fluid dynamics, Comput. Biol. Med. 38 (6) (2008) 713–726.

[11] F. Zare, et al., Targeted drug delivery to the inferior meatus cavity of the nasal airway using a nasal spray device with angled tip, Comput. Methods Prog. Biomed. 221 (2022), 106864.

[12] X. Tong, et al., Effects of nasal drug delivery device and its orientation on sprayed particle deposition in a realistic human nasal cavity, Comput. Biol. Med. 77 (2016) 40–48.

[13] F.R. Menter, Two-equation eddy-viscosity turbulence models for engineering applications, AIAA J. 32 (8) (1994) 1598–1605.

[14] ANSYS, I. ANSYS FLUENT 12.0 theory guide. 2009 [cited 2023 03/08]; Available from: https://www.afs.enea.it/project/neptunius/docs/fluent/html/th/node67.htm.

[15] J. Dong, et al., Numerical comparison of nasal aerosol administration systems for efficient nose-to-brain drug delivery, Pharmaceut. Res. 35 (1) (2017) 5.

[16] K. Shrestha, et al., Effect of breathing profiles on nebuliser drug delivery targeting the paranasal sinuses in a post-operative nasal cavity, J. Aerosol. Sci. 161 (2022), 105913.

[17] H. Calmet, et al., Validation and Sensitivity analysis for a nasal spray deposition computational model, Int. J. Pharmaceut. 626 (2022), 122118.

[18] A.V. Kolanjiyil, et al., Validating CFD predictions of nasal spray deposition: inclusion of cloud motion effects for two spray pump designs, Aerosol Sci. Technol. 56 (4) (2022) 305–322.

[19] K. Inthavong, et al., Simulation of sprayed particle deposition in a human nasal cavity including a nasal spray device, J. Aerosol Sci. 42 (2) (2011) 100–113.

[20] J.D. Schroeter, G.J.M. Garcia, J.S. Kimbell, Effects of surface smoothness on inertial particle deposition in human nasal models, J. Aerosol Sci. 42 (1) (2011) 52–63.